Information Sciences Letters
An International Journal

http://dx.doi.org/10.18576/isl/130214

Effect of Adding Two Intermediate Oxides (Bi2O3 and MnO2) in Place of a Glass's Original Oxide (B2O3) on the Structural, Optical, and Shielding Qualities of Several Sodium Borate-based Glasses

Hosam M. Gomaa[1], H. A. Saudi[2,], A. M. Moneep[3], A. A. Bendary[3], Algendy S. Algendy[4], Ahmed. M. Mabrouk[4] and Takwa E. Ellakwa[5]*

[1] Pharaohs-Higher Institute, Giza, Egypt
[2] Physics Department, Faculty of Science, Al-Azhar University, (girls branch), Nasr City, Cairo, Egypt
[3] Physics Department, Faculty of Science, Al-Azhar University, Cairo, Egypt
[4] Architecture Department, Faculty of Engineering, Al-Azhar University, Nasr City, Cairo, Egypt
[5] Physical Chemistry Department, Faculty of Pharmacy, Egyptian Russian University, Cairo, Egypt

Received: 11 Oct 2023, Revised: 23 Nov. 2023, Accepted: 1 Dec. 2023.
Published online: 1 Mar. 2023

Abstract: This work prepared a set of six samples of sodium borate glass containing different concentrations of bismuth and manganese cations using the rapid cooling method. In addition to molar volume calculations, measurements of density, X-ray patterns, and infrared spectra confirmed the amorphous nature of all samples and that the lower B2O3 content sample has the highest homogeneity of all samples. FTIR revealed many structural units throughout the glass networks, like BO3, BO4, BiO3, and BiO6. The replacement of B2O3 by both Bi2O3 and MnO forced BO3 units to convert to BO4 units, causing an increase in the number of nonbridging oxygen atoms. It also forces BiO3 units, which are glass network formers, to convert to BiO6 units, which act as glass network modifiers and occupy the interstitial vacancies. The replacement of B2O3 by both Bi2O3 and MnO caused an increase in the glass bulk density, the glass molar volume, the number of nonbridging oxygen atoms, and the density of the localized states. It also increased the values of the optical reflectance, absorption coefficient, refractive index, absorption index, and mass attenuation coefficient. On the other side, such a replacement caused a decrease in the values of the optical band gaps and the half-value layer. The study results suggest the investigated samples are perfect cathode glasses. It also nominates the sample with the lowest B2O3 content for gamma ray shielding applications and vice versa for neutrons.

Keywords: Borate glass, Oxide glass, Shielding, Optical properties, Homogeneous glasses.

1 Introduction

Borate glasses have a wide variety of applications and offer varying physical and chemical properties by changing the chemical composition. Boron can change its coordination with oxygen between three or four. Hence, it forms variable structural units in the glass network, and such behavior is quite different than that of silicon and phosphorous, which constitutes only tetrahedral coordinated units with oxygen. Borate glasses have been extensively studied as a glass-forming system [1-2]. Mainly, borate glasses are having so many potential applications like thin amorphous films for battery applications, bioactive glasses for tissue engineering, nuclear waste disposal, photonic applications, development of tunable or short pulse lasers, optical fiber amplifiers and fiber lasers etc. [3–8]. Among oxide glasses, borate glass structures have disordered geometry with the formation of tetrahedral coordination of BO4 units. Sodium oxide (Na2O) and boron trioxide (B2O3) are the major components of many industrial important glasses [9]. The main application of these glasses ranges from cookware to laboratory glassware to optical glass [10, 11]. Because of this reason, many glass researchers have conducted structural physical studies to understand how the density molar mass of each oxide affects the glass network structure. Bi2O3-based glass possesses low melting temperature, big mass and high polarizable Bi3+ ions. Their relatively low phonon energy, high refractive index, high dielectric constant and good corrosion resistance are attractive in photonics and Magneto-optical (MO) devices [12–15]. B2O3 can modify Bi3+ into a vitreous network [16-18] since they cannot form glass alone. Manganese is one of the TMs with color and can be considered a catalyst or sensitizer in various glasses and crystals [19-21]. In glasses, manganese is predicted to be Mn2+, Mn3+, Mn4+, MnO4−, and MnO42− ions or a mixture. Depending on the host materials, the Mn2+ ion is luminescent with many visible lights, including green light, yellow light, and red-light emission [22-25]. Lately, Gaddam et al. found that Mn acts as a network modifier or network former and confirmed the presence of Mn3+ in the

*Corresponding author e-mail: Heba_Saudi@azhar.edu.eg

oxidation equilibrium of Mn2+/ Mn3+ in the following glass system [26-27]. Accordingly, this work aims to estimate the impact of Bi3+ and Mn4+ Impurities on the pure sodium borate-based glass's structural, optical, and shielding parameters.

2 Experimental methods

A set of six glass samples have been suggested according to the chemical formula, (75-x) mol%B2O3 – 25mol% Na2O – x mol % (0.1 MnO2 - 0.9 Bi2O3), where =here x = 0, 5, 10, 15, 20 and 25. The components of each sample were weighted in a mole percentage approach, and then they were mixed in a porcelain crucible. Finally, all samples were transferred into an electric furnace, with a temperature of about 1400 oC, for two an hour before they had quenched in the air between two copper plates. The internal structure of the obtained solid samples was characterized by inspecting the spectral charts of both XRD and FTIR, where the XRD measurements were obtained by a Burkeraxs d8 advance type X-ray diffractometer with Cu ka of 0.1541 nm radiation. In contrast, The FTIR absorption spectra were received by the KBr pellets technique at RT in a wavenumber range of 400-4000 cm-1 using a CARY 630 FTIR spectrometer. The density (ρ) was measured using the Archimedes technique at RT using Toluene as an immerging liquid with a density of (0.864 g/cm3). The molar volume was then calculated using Vm = M/ρ (where M is the molecular weight). The glass samples' optical transmittance and reflectance spectra were recorded at RT in the wavelength range of 190-1100 nm using a Shimadzu UV-3600 UV-Vis-Nir spectrophotometer. The measured samples were cut and polished carefully before performing optical measurements.

3 Results and discussion

3. 1 Characterization of samples structures:

The bulk density of solid material is one of the easily primary powerful tools that can be affected by any change in the internal structure of this material, even if it is hyperfine. Because the bulk density increases monotonically with the degree of crystallinity, the density value of a solid sample in its crystalline form is greater than that of the same sample in its amorphous form. As seen in Figure 1, the densities of the prepared samples have been measured and compared with the calculated values to check the deviation in crystallinity degree. The apparent increase in measured and calculated densities can be attributed to the exchange of B2O3 (69.62 g) with 0.1 M and 0.9 Bi2O3 (428.06 g/mol). The difference between the calculated and measured densities for each sample indicates that the prepared samples are amorphous due to the short-range order in their structures.

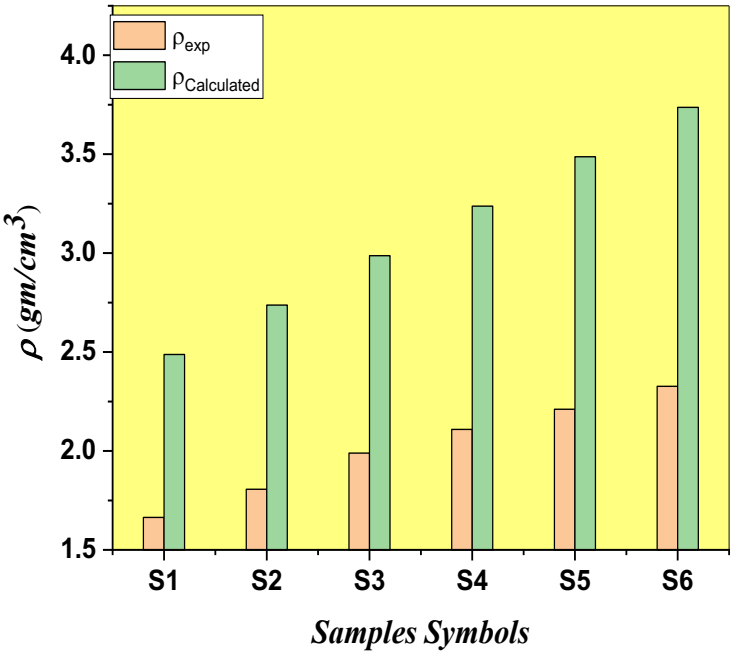

Fig. 1: Measured and calculated densities of the prepared samples

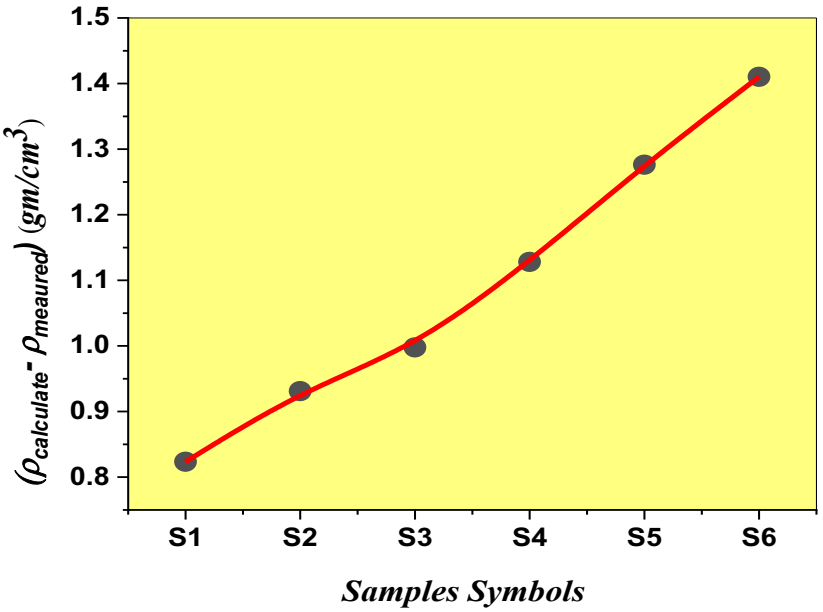

Fig. 2: Difference between the measured and calculated densities of the prepared samples

Figure 2 reveals that the difference between the measured and calculated densities increased when MnO and Bi_2O_3 replaced B_2O_3. This observation could imply that sample S6, which has the lowest B_2O_3 content, has the highest disordering degree of all the samples. Such conclusions were confirmed by another more accurate and powerful tool, X-ray diffraction XRD, in the characterization of the internal structure of the solid materials, where the XRD patterns differ depending on the internal matrix of the solid. XRD patterns display sharp peaks for crystalline substances, whereas amorphous solids may indicate one or more wide humps. Therefore, XRD imaging was performed on each of the samples under investigation.

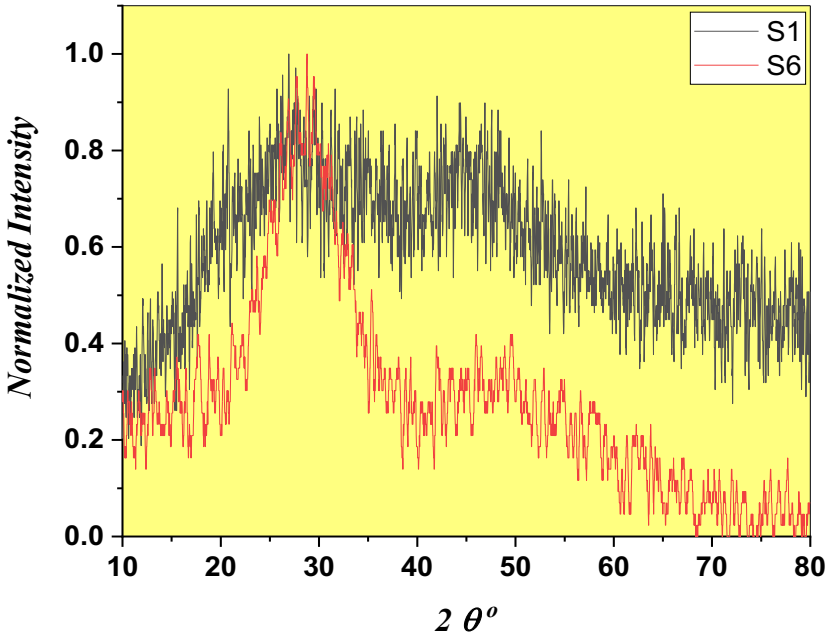

Fig. 3: X-ray diffraction XRD patterns for all samples

As shown in Figure 3, all samples displayed just two humps that varied in relative intensity and bandwidth. An absence of sharp peaks confirms the amorphous phases (short-range order structures) of the prepared samples, while the decrease in the enclosed area confirms the increase in the amorphous degree when B_2O_3 was replaced by both MnO and Bi_2O_3. Accordingly, according to the density measurements and X-ray patterns, in addition to the method of preparation, it can be said that the prepared samples have highly homogeneous glass states, and the degree of homogeneity also increases when B_2O_3 is replaced by both MnO and Bi_2O_3. The molar volume (Equation 1 [28], Figure 4) has been calculated as a tool for determining whether or not the glass is homogeneous. Where, it's well known that a glass with high homogeneity should have a large molar volume, and vice versa [29-30].

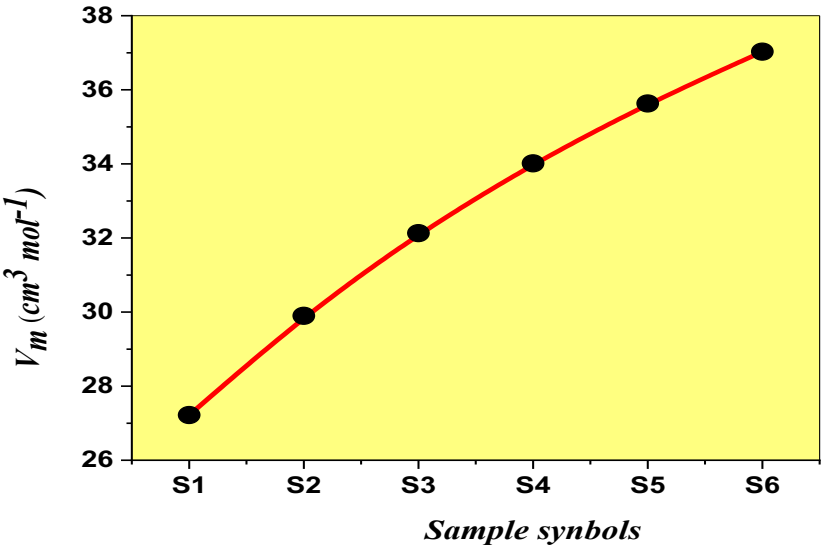

Fig. 4: Molar volumes of the studied samples

Such a procedure has been performed to eliminate confusion caused by increased density values and glass homogeneity. As shown in Fig. 4, sample S6 (with the lowest B_2O_3 content) has the largest molar volume, which reveals its high homogeneity.

$$V_m = \frac{\sum M_i}{\rho} \quad (cm^3\ mol^{-1}) \tag{1}$$

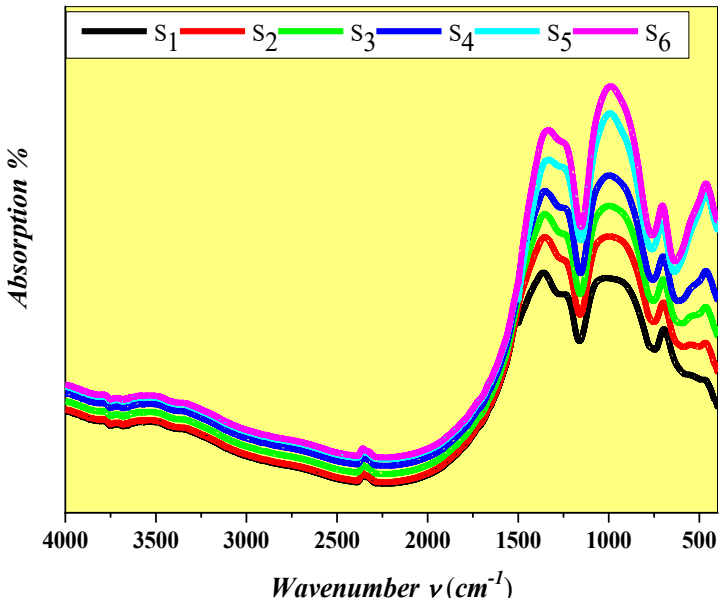

Fig. 5a: Fourier transform infrared FTIR charts for all samples

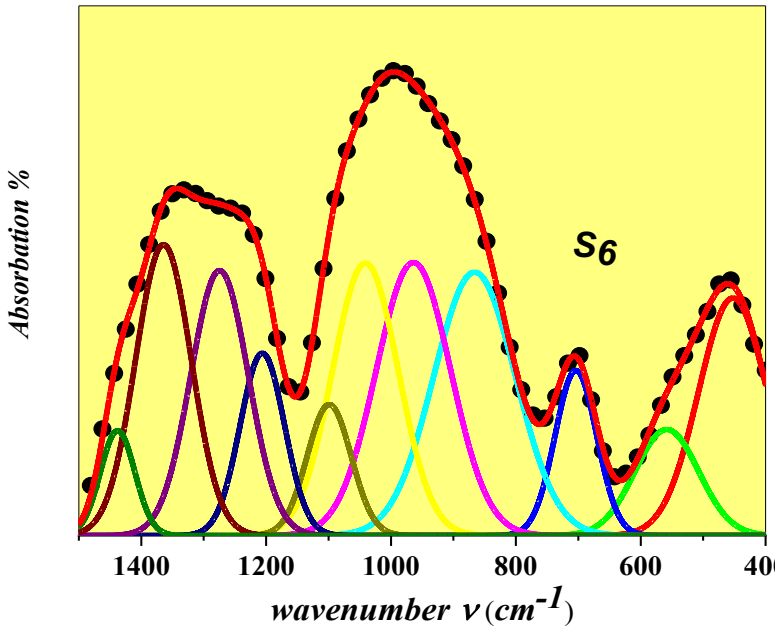

Fig. 5b: Fourier transform infrared FTIR deconvoluted spectrum for sample S_6

Figure 5a depicts the collected Fourier transform infrared FTIR spectra for the studied samples in the 4000-400 cm^{-1} range. Based on the Gaussian distribution function, the FTIR chart of each sample was deconvolution to some of the individual peaks, where each characterized a certain vibration of a special structural group unit or chemical bond, as seen in Figure 5b for sample S6 in the range 1500-400 cm^{-1}. The detected peaks were assigned to their vibrators based on the related previously published studies, as seen in Table (1) [31-40]. The deconvolution process increased the vibration of BO_2-O-BO_3, which means an increase in the non-bridging oxygen atoms, which confirms the increase in the glass homogeneity (randomness) as B_2O_3 decreases. Also, it was found that Bi cation was incorporated into the glass network as BiO_3 and BiO_6, with an increase in the vibration intensity of BiO_6 at the expense of BiO_3, which explains the increase in glass bulk density.

Table 1: FTIR peaks assignments:

Peak	Assignments	Refs.
446	the bending vibration of Bi-O bonds in BiO_3 polyhedral [17], and/or the vibration of structural deformations	[31-40]
557	the vibrations of the Bi–O bonds in the BiO_6 octahedral unit [7-9], with the bands of the in-plane bending vibration of BO_3 units	
703	Belong the bending vibration of B-O-B in BO_3 triangles. The intensity of this band increases with the gradual increase of Bi_2O_3.	
794	the vibration modes of the Mn–O– Mn bonding in a-MnO_2 nanorods	
965 1099	B-O stretching vibration of tetrahedral BO_4 units from pentaborate groups.	
1207	B-O symmetric stretching vibration of trigonal BO_3 units [2, 18], and/or B-O bond stretching vibrations and B-O bridging between B_3O_6 rings and BO_3 triangles.	
1276	the asymmetric stretching vibration of B–O bond in BO_3 trigonal units.	
1363 1436	B–O stretching vibration $(BO_3)^{3-}$ units in meta-borate and ortho-borates chains	

3.2 Optical & shielding characterization:

The optical reflectance spectra of the examined samples are shown in Figure 6, "reflectance" is the proportion of incident flux to reflected radiant optical power at a reflecting sample. Generally, the optical reflectance is influenced by the optical wavelength and incident light angle.

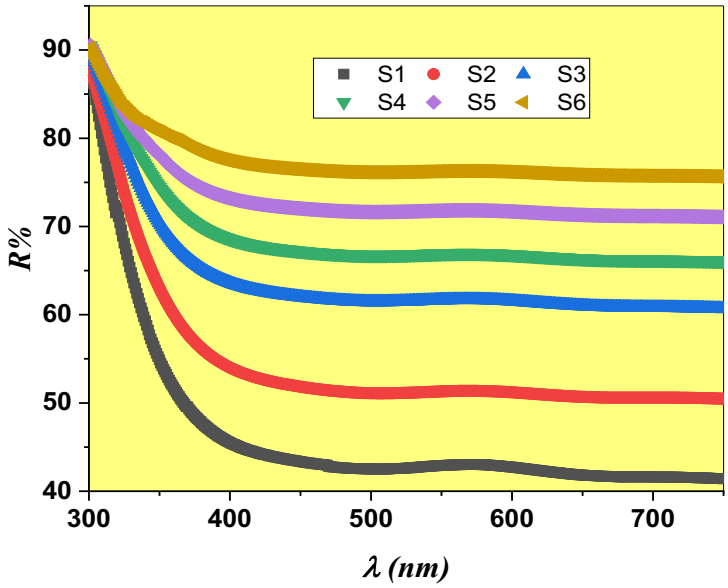

Fig. 6: Optical reflectance R% of all samples

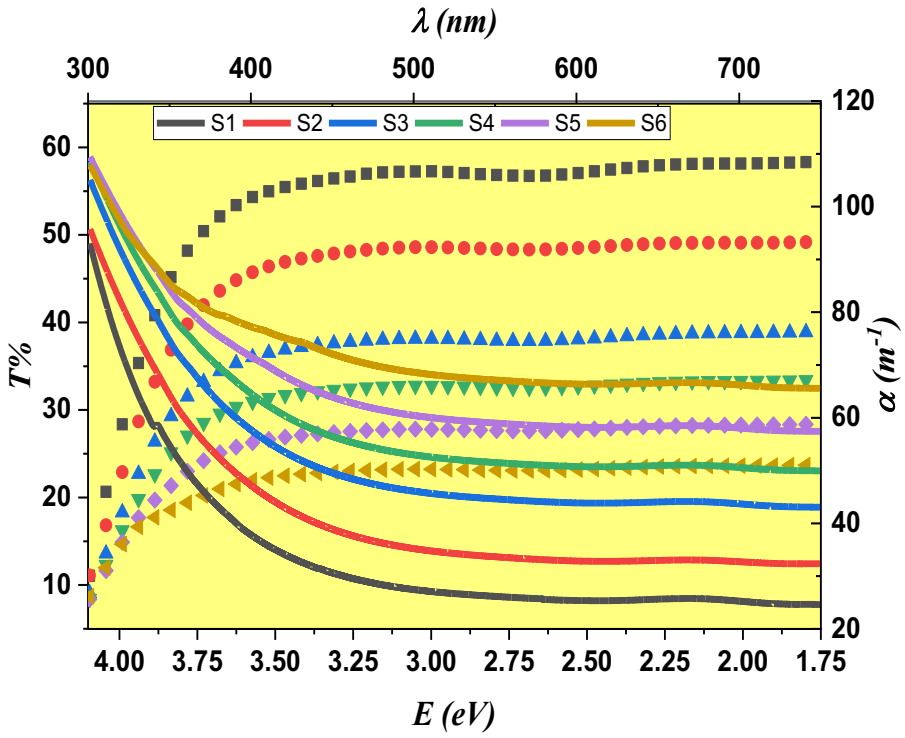

Fig. 7: Optical transmittance T% (dot lines) & Absorption Coefficient α (solid lines) for all samples

Figure 6 demonstrates that the reflectance value increased when B_2O_3 content decreased, which may be explained by an increase in the density of scattering reactions caused by the increase in the density of negative charge carriers (nonbridging oxygen atoms), particularly given that all samples are the same thickness. As shown in Figure 7, such a result was confirmed by the decrease in the optical transmittance T% value and the increase in the value of the optical absorption coefficient (which was calculated by using Equation 2, where t is the sample thickness)

$$.\alpha = 2.303 \frac{100-R\%-T\%}{t} \quad [41\text{-}42] \qquad (2)$$

$$\alpha = \frac{Constant}{E}\left(E - E_g\right)^{\gamma} \quad [41\text{-}42] \tag{3}$$

$$(Where\ \gamma = \frac{1}{2}\ for\ direct\ transitions\ \&\ \gamma = 2\ for\ indirect\ transitions)$$

$$n = \frac{1+\frac{R}{4}}{1-\frac{R}{4}} + \sqrt{\frac{R}{(1-\frac{R}{4})^2} - (K)^2} \quad \text{Linear refractive index} \quad [43] \tag{4}$$

$$K = \frac{\alpha\lambda}{4\pi}, absorption\ index \quad [43] \tag{5}$$

$$\alpha = Constant\ e^{\frac{E}{E_U}} \quad [41\text{-}42] \tag{6}$$

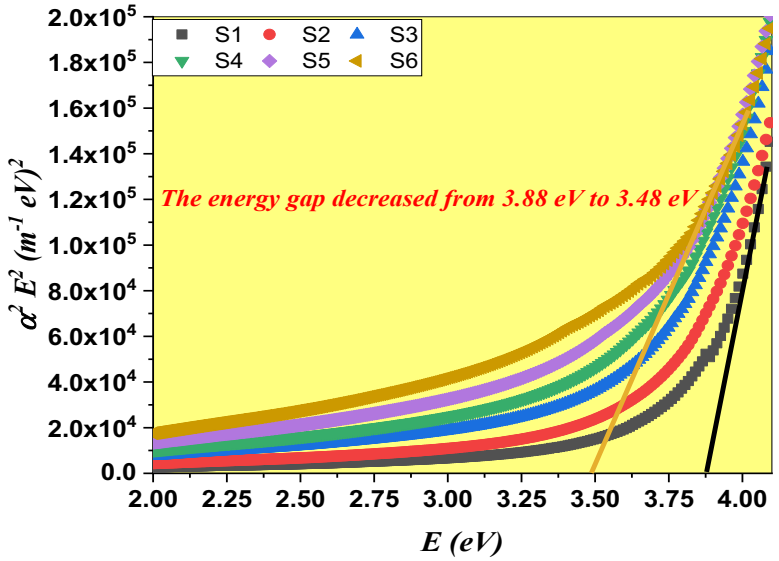

Fig. 8: Optical gap determination for direct transitions

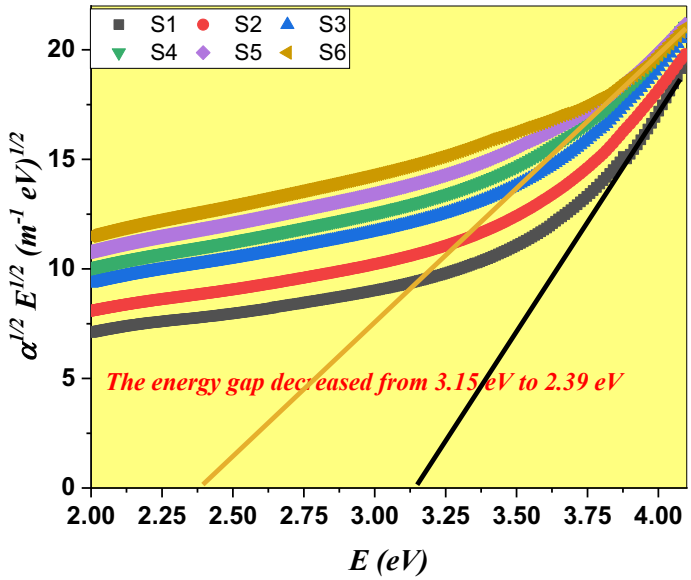

Fig. 9: Optical gap determination for indirect transitions

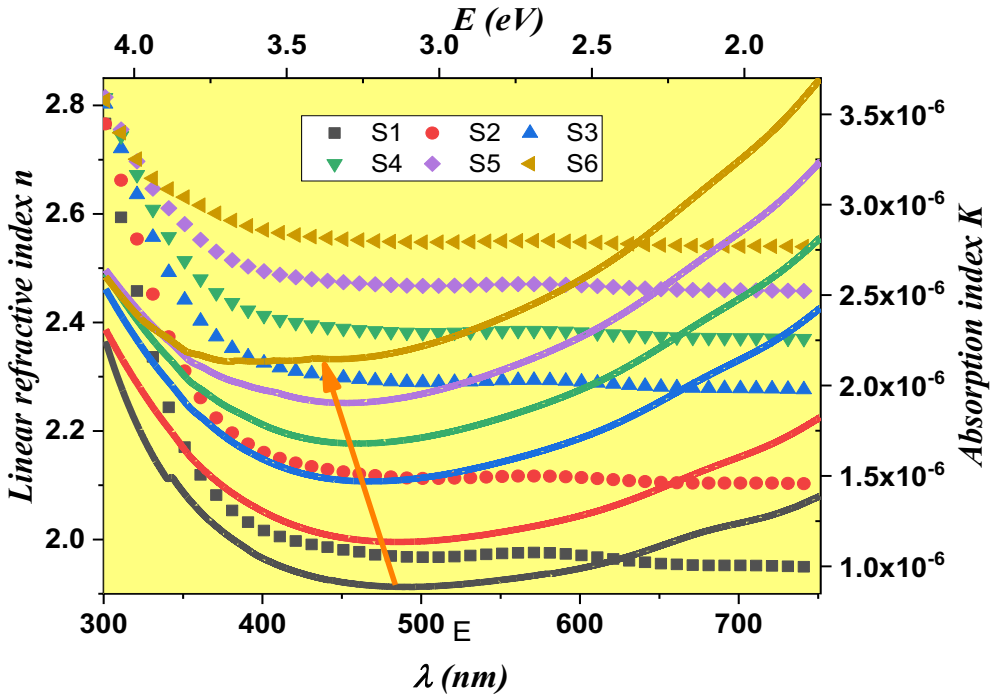

Fig. 10: Linear refractive indices n (dot lines) & Absorption indices K (solid lines) for all samples

The change in the absorption coefficient value indicates that as the B_2O_3 content decreases, a change in the electronic configurations within the glass networks is required, necessitating a change in the values of the energy gaps of the electronic transitions, whether direct or indirect. Accordingly, Tauc's approximation (Equation 3) has been used to estimate how the decrease in B_2O_3 content impacts the optical band gap values, as seen in Figures 8 and 9. It is clear that with the decrease in the B_2O_3 content, the energy gap values of direct and indirect electronic transitions are weighed down from 3.88 to 3.48 eV and from 3.15 to 2.39 eV, respectively, which explains the increase in the values of the absorption coefficient, especially since the samples have the same thickness. Such a decrease in the energy gaps, as well as the reported increase in optical reflectance, may explain the increase in the values of the absorption index K and the linear refractive index n, Figure 10, (that were calculated using Equations 4 and 5) [43]. The increase in the value of the absorption index may refer to an increase in the density of structural defects (localized states).

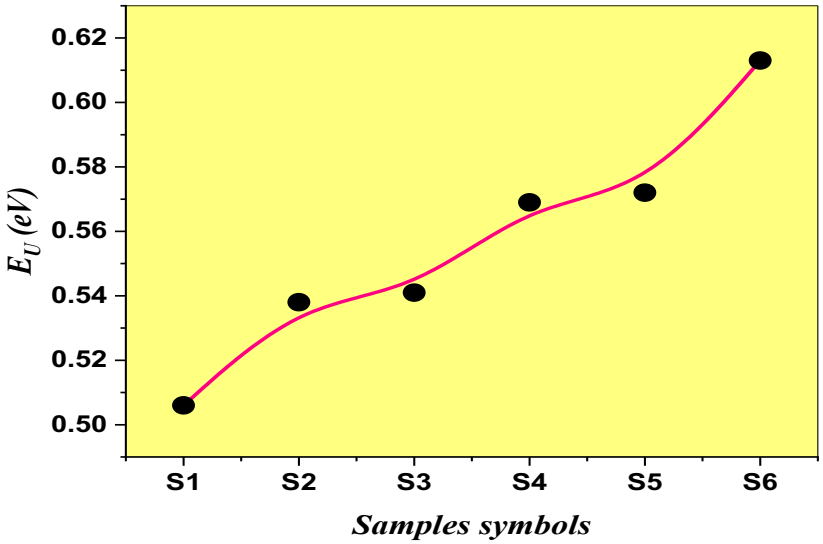

Fig. 11: Urbach's energies of the studied samples

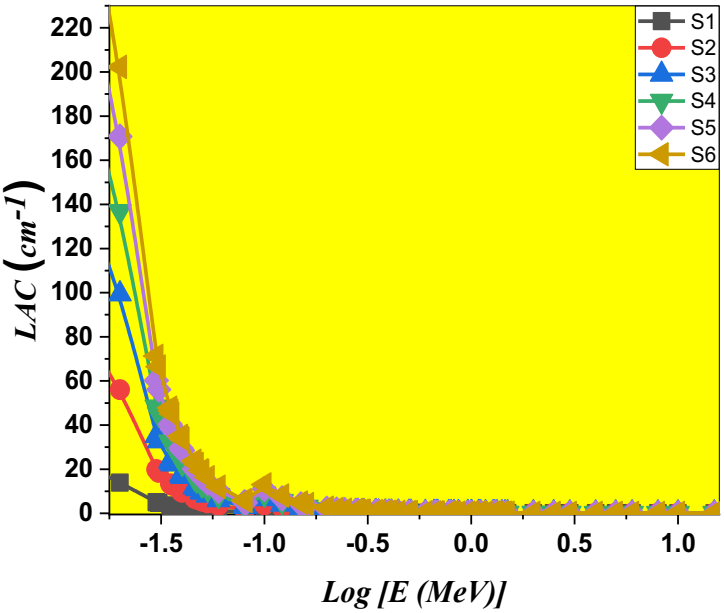

Fig. 12: The linear attenuation coefficients of the studied samples, at different energies

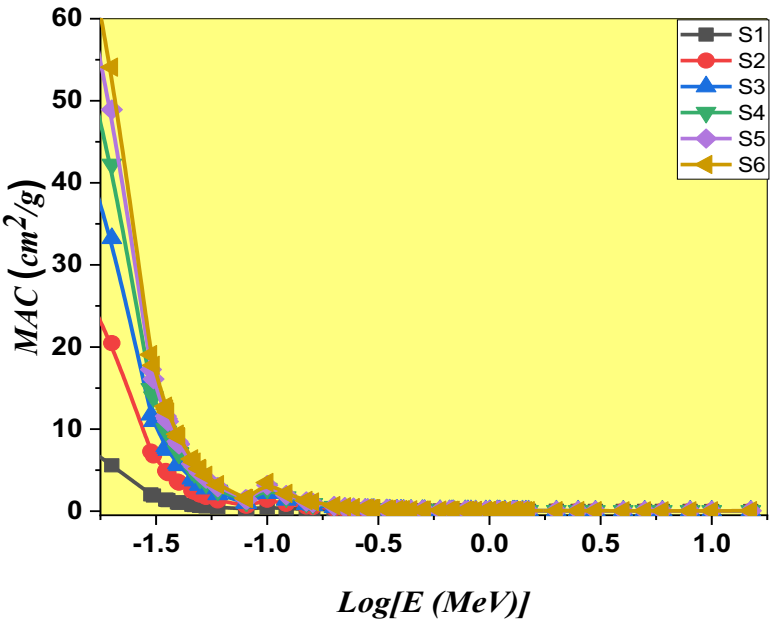

Fig. 13: The linear attenuation coefficients of the studied samples, at different energies

This conclusion was confirmed by calculating the Urbach's energies of all samples (Eq. 6), which showed an increase as B_2O_3 content decreased, see Figure 11. On the other hand, an increase in the linear refractive value n may nominate the sample S6 as a high-energy radiation attenuator, so the gamma attenuation parameters (linear and mass attenuation coefficient, HVL half-value layer, MFP average path value and Zeff effective atomic number) were calculated using WinXcom source software The common radioactive substances are ^{137}Cs, ^{133}Ba, ^{152}Eu and ^{60}Co (different energies), as shown in Figures 12 to 16. In Figures. 12, 13, and 14, the linear (LAC), mass attenuation coefficient (MAC)and the effective atomic number (Zeff) decreased with increasing energy. They increased with increasing MnO_2, Bi_2O_3, and B_2O_3 content decreased, while HVL and MFP showed the opposite in Figure 15 and 16. These results point to the fact

that the present samples provided radiation protection with decreased B_2O_3, which may be attributed to the increase of BiO_6 in the interstitial voids of the glass and the increase in the unannealed oxygen atoms. With the help of the NXCOM program [44-47], calculate the fast neutron removal cross-section (FNRCS) (1/cm) of the present glass system. The values of FNRCS for the current glass, as shown in Figure 17, indicate that the sample containing 75% boron oxide is the most attenuating of the fast neutrons due to the high cross-sectional area of the boron. The decrease in neutron attenuation with the increase in bismuth and manganese oxides is due to an increase in non-bridged oxygen atoms and an increase in the homogeneity of the glass (randomness), which is consistent with the results of IR.

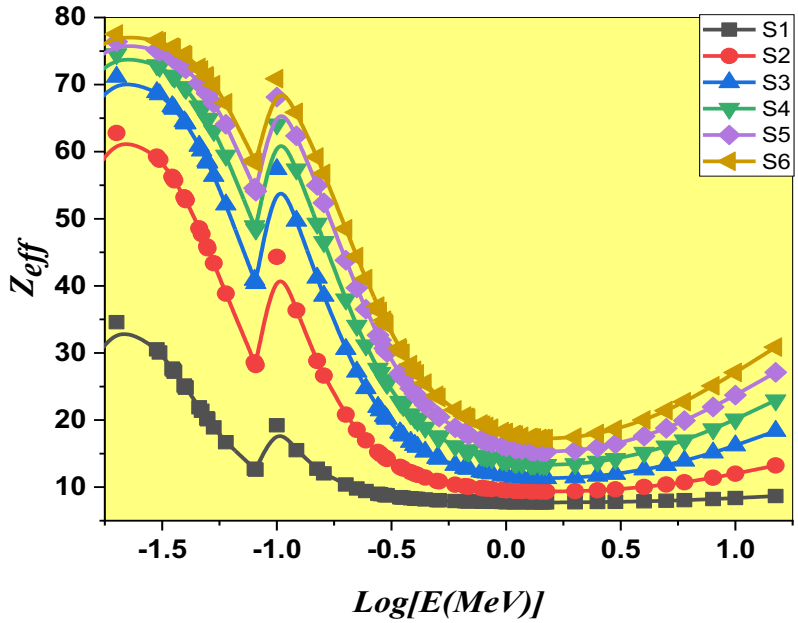

Fig. 14: The Z_{eff} of the studied samples, at different energies

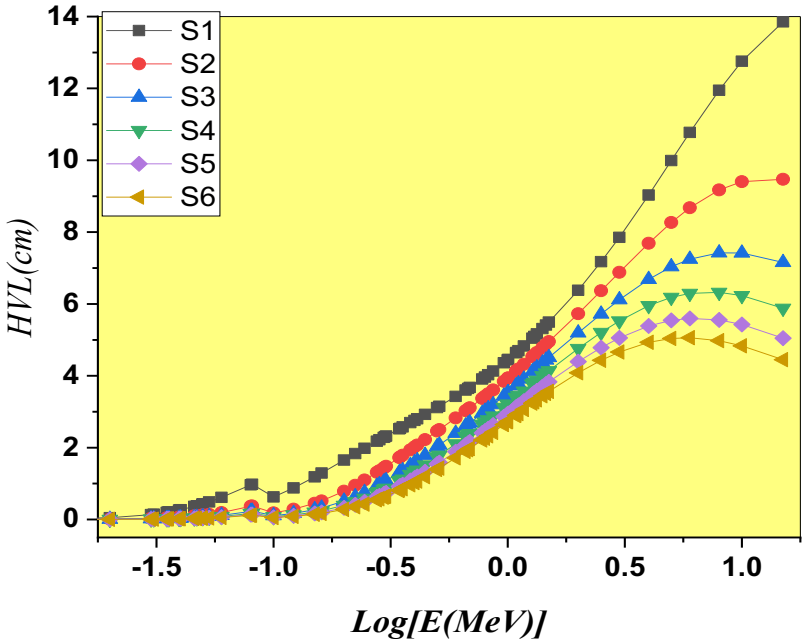

Fig. 15: The HVL of the studied samples, at different energies

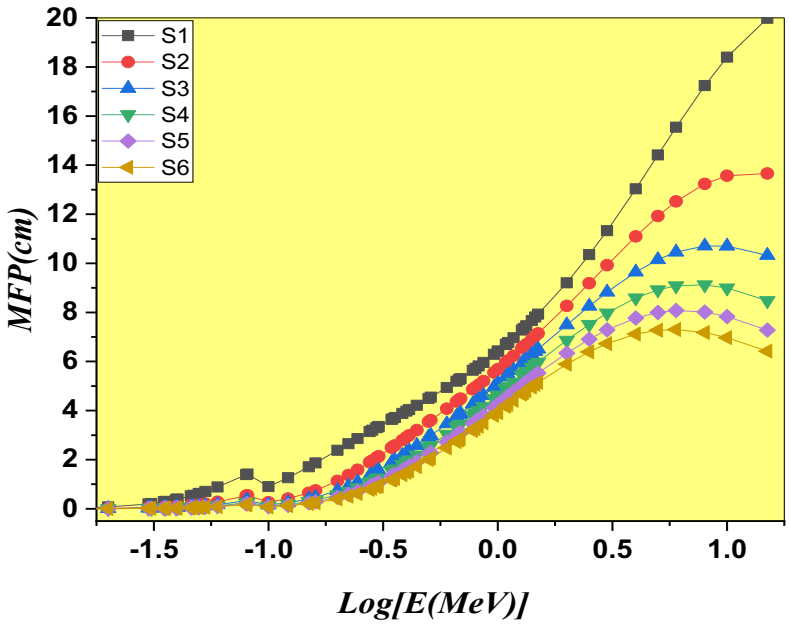

Fig. 16: The HVL of the studied samples, at different energies

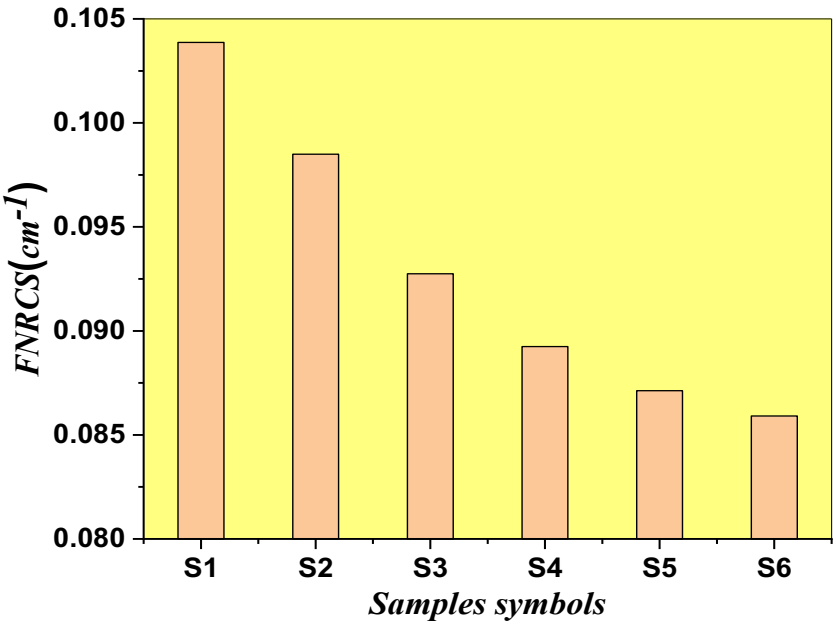

Fig. 17: The FNRCS of the studied samples

4 Conclusions

The glass system of (75-x) mol%B2O3 – 25mol% Na2O – x mol% (0.1 MnO2 - 0.9 Bi2O3), where here x = 0, 5, 10, 15, 20 and 25 has been examined for its physical, optical, and radiation shielding capabilities. The investigation led to the following conclusion: The density of the glasses increases with increasing MnO2 - Bi2O3 content because MnO2 - Bi2O3 have larger molecular weight than B2O3. The glass's molar volume increases as the amount of MnO2 - Bi2O3 increases, indicating that the MnO2 - Bi2O3 functions as a modifier in the glass network. Results of FTIR revealed

several structural units such as BO3, BO4, BiO3 and BiO6. The replacement of B2O3 with Bi2O3 and MnO converted BO3 into BO4 units, causing an increase in the number of unconjugated oxygen atoms. BiO3 units are also converted to BiO6 units, which act as modifiers of the vitreous lattice and occupy interstitial vacancies. Replacing B2O3 with both Bi2O3 and MnO increased the values of optical reflectance, absorption coefficient, refractive index, and linear mass attenuation coefficient. On the other hand, this substitution caused lower optical bandgap values, a half-value layer and a mean free path. All the results prove that the samples examined are perfect cathode glasses. Also, the sample with the lowest B2O3 content can be used for gamma-ray shielding applications and vice versa for neutrons.

5 Declarations

Ethical Approval: This article doesn't contain any studies involving animals performed by any authors. Also, this article does not have any studies involving human participants performed by any of the authors.

Authors' contributions:

Hosam M. Gomaa performed all calculations, data analysis, and wrote the sections of abstract as well as results and discussion except the shielding part. H. A. Saudi wrote the shielding section and conclusion. A M moneep and A.A bendary performed the experimental measurements and wrote the introduction and experimental sections. M. Y. Hassan reviewed the final manuscript.

Funding: Not applicable

Data Availability Statement: All the original measurements and data analysis of this work will be available when required.

Conflicts of Interest Statement

The authors certify that they have NO affiliations with or involvement in any organization or entity with any financial interest (such as honoraria; educational grants; participation in speakers' bureaus; membership, employment, consultancies, stock ownership, or other equity interest; and expert testimony or patent-licensing arrangements), or non-financial interest (such as personal or professional relationships, affiliations, knowledge or beliefs) in the subject matter or materials discussed in this manuscript.

References

[1] G. Kaur, et al., (2014). A review of bioactive glasses: their structure, properties, fabrication and apatite formation, J. Biomed. Mater. Res. A 102 (1): 254–274. https://doi.org/10.1002/jbm.a.34690.

[2] A. K. Varshneya, Fundamentals of Inorganic Glasses, Elsevier, 2013.

[3] Górny, A., Kuwik, M., Pisarski, W. A., & Pisarska, J. (2019). Lead Borate Glasses and Glass-Ceramics Singly Doped with Dy3+ for White LEDs. *Materials*, *13*(21), 5022. https://doi.org/10.3390/ma13215022H.

[4] Gomaa, H. M., Moneep, A., Bendary, A., Yahia, I., & Zahran, H. (2022). Structural and optical absorption coefficient analysis of barium lead sodium-borate glass doped with graphene nanopowder. Optik, 271, 170090. https://doi.org/10.1016/j.ijleo.2022.170090.

[5] S. K. Arya, S. S. Danewalia, K. Singh (2016). Frequency independent low-k lithium borate nanocrystalline glass ceramic and glasses for microelectronic applications, J. Mater. Chem. C 4 (15) : 3328–3336. https://doi.org/10.1039/C5TC03364K.

[6] K. Annapoorani, Ch. Basavapoornima, N. Suriya Murthy, K. Marimuthu, (2016). Investigations on structural and luminescence behavior of Er3+ doped Lithium Zinc borate glasses for lasers and optical amplifier applications, J. Non-Cryst. Solids 447 273–282.https://doi.org/10.1016/j.jnoncrysol.2016.06.021.

[7] E. M. Masoud, M. Khairy, M.A. Mousa (2013). Electrical properties of fast ion conducting silver based borate glasses: application in solid battery, J. Alloys Compd. 569 150–155. http://dx.doi.org/10.1016/j.jallcom.2013.03.113.

[8] Mohsen H.Abdel-Wahed, Saleh M. Abdou, A. S. El-Bayoumi, S. M. Salem, A. A. Bendary (2020). Structural, optical properties and γ - ray shielding parameters of PbO embedded Li2O borophosphate glass systems, J. Non-cryst. Solids 543: 120135.http://dx.doi.org/10.1016/j.jnoncrysol.2020.120135.

[9] S. Mohan, K.S. Thind (2016). Investigation of luminescence and spectroscopic properties of Nd3+ ions in

cadmium alkali borate glasses, Opt. Mater. 57 :134–139.https://doi.org/10.1016/j.optmat.2016.04.040.

[10] Marina Barlet, Ali Kerrache, Jean-Marc Delaye, Cindy L.Rountree (2013). SiO2–Na2O–B2O3 density: a comparison of experiments, simulations, and theory, J. Non-Cryst. Solids 382: 32–44. http://dx.doi.org/10.1016/j.jnoncrysol.2013.09.022.

[11] Mahesh M. Hivrekar, D. B. Sable, M. B. Solunke, K. M. Jadhav (2017). Network structure analysis of modifier CdO doped sodium borate glass using FTIR and Raman spectroscopy, J. Non-Cryst. Solids 474: 58-65. http://dx.doi.org/10.1016/j.jnoncrysol.2017.08.028.

[12] Hongtao Sun, Lei Wen, Shiqing Xu, Shixun Dai, Lili Hu, Zhonghong Jiang (2005) Novel lithium-barium-lead-bismuth glasses, Mater. Lett. 59: 959–962. https://doi.org/10.1016/j.matlet.2004.09.051.

[13] Y. Cheng, H. Xiao, W. Guo, W. Guo (2007). Structure and crystallization kinetics of PbO-B2O3 glasses, Ceram. Int. 33: 1341–1347. https://doi.org/10.1016/J.CERAMINT.2006.04.025.

[14] Qiuling Chen, Chao Wu, Shiyu Yin, Qiuping Chen (2012). Accurate Faraday measurement system for PBB glasses in current transducer application, Adv. Mater. Res. 476–478. https://doi.org/10.4028/www.scientific.net/AMR.476-478.498.

[15] Prasad, R., Siva, B.V., Neeraja, K., Mohan, N.K., & Rojas, J.I. (2020). Influence of modifier oxides on spectroscopic features of Nd2O3 doped PbO-Ro2O3–WO3–B2O3 glasses (with Ro2O3 = Sb2O3, Al2O3, and Bi2O3). Journal of Luminescence.https://doi.org/10.1016/J.JLUMIN.2020.117171.

[16] Mahmoud, K., Abdel-Rahim, F., Atef, K., & Saddeek, Y. (2010). Dielectric dispersion in lithium–bismuth-borate glasses. Current Applied Physics, 11(1), 55-60.https://doi.org/10.1016/j.cap.2010.06.018.

[17] Srisittipokakun, N., Kaewkhao, J., Chewpraditkul, W., & Limsuwan, P. (2011). Comparative Study of Optical and Spectroscopic Properties of Lead and Bismuth on Borosilicate Glasses. Procedia Engineering, 32, 699-705. https://doi.org/10.1016/j.proeng.2012.01.1329Qiuling Chen,

[18] Qiuping Chen, Hui Wang, Gaimin Wang, Shuai Yin (2017). Magneto optical properties of rare earth Tb2O3 doped PbO-Bi2O3-B2O3 glass, J. Non-cryst. Solids 470 : 99-107.https://doi.org/10.1016/J.JNONCRYSOL.2017.05.008.

[19] Kh.S. Shaaban, Nissren Tamam, Hawra A. Alghasham, Z.A. Alrowaili, M.S. Al-Buriahi, Takwa E. Ellakwa, Thermal, optical, and radiation shielding capacity of B2O3-MoO3-Li2O- Nb2O5 glasses,Materials Today Communications,Volum37,2023,107325,https://doi.org/10.1016/j.mtcomm.2023.107325.

[20] X. J. Wang, D. D. Jia, W.M. Yen (2003). Mn+2 activated green, yellow, and red long persistent phosphors, J. Lumin 103 (2003) 34–37. https://doi.org/10.1016/S0022-2313(02)00541-0.

[21] P. Kupracz, J. Karczewski, M. Prze´sniak-Welenc, N. A. Szreder, M.J. Winiarski, T. Klimczuk, R.J. Barczy'nski (2015). Microstructure and electrical properties of manganese borosilicate glasses, Journal of Non-Crystalline Solids 423–424 (2015) 68–75. https://doi.org/10.1016/j.jnoncrysol.2015.05.014.

[22] A. Winterstein-Beckmann, D. Moncke, D. Palles, E.I. Kamitsos, L. Wondraczek, Structure–property correlations in highly modified Sr, Mn-borate glasses, J. Non Cryst. Solids 376 (2013) 165–174. https://doi.org/10.1016/j.jnoncrysol.2013.05.029.

[23] D. Moncke, ¨ E.I. Kamitsos, A. Herrmann, D. Ehrt, M. Friedrich (2011). Bonding and ion–ion interactions of Mn2+ ions in fluoride–phosphate and boro-silicate glasses probed by EPR and fluorescence spectroscopy, J. Non-Cryst. Solids 357 (14) : 2542–2551. https://doi.org/10.1016/j.jnoncrysol.2011.02.017.

[24] A. Terczyn'ska-Madej, K. Cholewa-Kowalska, M. Łaczka, The effect of silicate network modifiers on colour and electron spectra of transition metal ions, Opt. Mater. 32 (11) (2010) 1456–1462. https://doi.org/10.1016/j.optmat.2010.05.024.

[25] S. P. Singh, Aman, A Tarafder (2004). Comparative investigation on the effect of alkaline earth oxides on the intensity of absorption bands due to Cu2+, Mn3+ and Cr3+ ions in ternary silicate glasses, Bulletin of Materials Science 27 (3) (2004) 281–287.https://doi.org/10.1007/BF02708518.

[26] WEYL W. A., Coloured glasses, Monographs of Glass Technology, edited by W. E. S. Turner (Society of Glass Technology, Sheffield, (1951).

[27] A. Gaddam, H. R. Fernandes, D. U. Tulyaganov, M. J. Pascual, J. M. F. Ferreira (2014) Role of manganese on the structure, crystallization and sintering of non-stoichiometric lithium disilicate glasses, RSC Adv. 4 : 13581–

13592. https://doi.org/10.1039/C3RA46393A.

[28] A. A. Abul-Magd, H.Y. Morshidy, A.M. Abdel-Ghany (2020). The role of NiO on the structural and optical properties of sodium zinc borate glasses, Opt. Mater. (Amst)., 109, 110301. doi: https://doi.org/10.1016/j.optmat.2020.110301.

[29] A. K. Varshneya and J. C. Mauro (2019). Fundamentals of Inorganic Glasses, Third Edition. https://doi.org/10.1016/C2017-0-04281-7.

[30] Andanov, P.. "Physics of amorphous materials by S. R. Elliott." (1985).

[31] Ardelean and M. Toderas (2006). "FTIR Structural Investigation of 3 B2O3?BaO Glass Matrix Containing Manganese ions," Advanced Materials for Optics and Electronics, Vol. 8, No. 3, p. 1118.

[32] Hashem, Ahmed M., A. Abdel-Latif, Hanaa M Abuzeid, H. Abbas, Helmut Ehrenberg, Rabie Saad Farag, Alain Mauger and C. M. Julien (2011) "Improvement of the electrochemical performance of nanosized α-MnO2 used as cathode material for Li-batteries by Sn-doping." Journal of Alloys and Compounds 509: 9669-9674. https://doi.org/10.1016/j.jallcom.2011.07.075.

[33] Cheng, Y., Xiao, H.N., Guo, W.M. and Guo, W.M. (2006) Structure and Crystallization Kinetics of Bi2O3-B2O3 Glasses. Thermochimica Acta, 444, 173-178. http://dx.doi.org/10.1016/j.tca.2006.03.016.

[34] Pal, I., Agarwal, A., Sanghi, S. and Aggarwal, M.P. (2011) Structural, Absorption and Fluorescence Spectral Analysis of Pr3+ Ions Doped Zinc Bismuth Borate Glasses. Journal of Alloys and Compounds, 509, 7625-7631.http://dx.doi.org/10.1016/j.jallcom.2011.04.114.

[35] Gomaa, H.M., Yahia, I.S., Makram, B.M.A. et al. (2021) Optical and structural studies of some zinc calcium borate glasses for optoelectronic device applications. J Mater Sci: Mater Electron 32, 9392–9399. https://doi.org/10.1007/s10854-021-05602-5.

[36] Gomaa, H.M., Saudi, H.A., Yahia, I.S. et al. (2021). Impact of graphite impurities on the structure and optical properties of the sodium borate oxide glass. J Mater Sci: Mater Electron 32, 27553–27563. https://doi.org/10.1007/s10854-021-07130-8.

[37] Kamil, S.M., Gomaa, H.M., El-Gammal, W. et al. (2021). Effect of exchanging PbO with NiO on the structure and optical parameters action of some lanthanum borate oxide glasses. J Mater Sci: Mater Electron 32, 24168–24175.https://doi.org/10.1007/s10854-021-06882-7.

[38] Gomaa, H.M., Saudi, H.A., Yahia, I.S. et al. (2022). Enhanced the optical, electrical, and shielding properties of some alkali-borate glasses doped with lanthanide cerium oxide, CeO2. J Mater Sci: Mater Electron 33, 3284–3296.https://doi.org/10.1007/s10854-021-07529-3.

[39] M. K. El-Mansy, Hossam Mohamed Gomaa, N. Hendawy, A. Sabry Morsy (2018). Effect of exchange of Bi+3 b y Nb+5 on the structural and optical properties of some (BBiNb)2 O7 CaO oxide glasses, Journal of Non-Crystalline Solids, Volume 485: P42-46. https://doi.org/10.1016/j.jnoncrysol.2018.01.036.

[40] Hossam M. Gomaa (2018). Influence of Bi2O3 on the physical and electrical properties of some Boro-Iron glasses, Journal of Non-Crystalline Solids, Volume 481, Pages 51-58, ISSN 0022-3093. https://doi.org/10.1016/j.jnoncrysol.2017.10.012.

[41] Hosam M. Gomaa, I.S. Yahia, H.Y. Zahren, H.A. Saudi, Ahmed H. El-Dosokey (2022). Effect of replacement of SiO2 with BaTiO3 on the cadmium calcium-borate glass: Aiming to obtain an active glass for optical and shielding applications, Radiation Physics and Chemistry, Volume 193,109955, ISSN 0969-806X.https://doi.org/10.1016/j.radphyschem.2021.109955.

[42] Gomaa, H.M., Yahia, I.S., Yousef, E.S. et al. (2022). A Novel Correction Method Toward Extraction of Reflectance and Linear Refractive Index of Some Borosilicate Glasses Doped with BaTiO3. J. Electron. Mater. 51: 6347–6355.https://doi.org/10.1007/s11664-022-09858-3.

[43] Gomaa, H.M., Yahia, I.S. (2022). Toward a novel and accurate relationship between electrical and optical conductivity in opto-material sciences: New strategy. J Comput Electron. https://doi.org/10.1007/s10825-022-01943-4.

[44] Hosam M. Gomaa, Ashraf A. Abul-Magd, Ahmad S. Abu-Khadra, I.S. Yahia, H.Y. Zahran (2022). Structural, and optical characterizations of Cu/Fe@Na2B4O7 oxide glass: For shielding and optical applications, Optik, Volume 261, 169170, ISSN 0030-4026. https://doi.org/10.1016/j.ijleo.2022.169170.

[45] A. M. El-Khayatt, NXcom (2011). A program for calculating attenuation coefficients of fast neutrons and gamma-rays, Ann. Nucl. Energy. 38 128–132.https://doi.org/10.1016/j.anucene.2010.08.003.

[46] Laifi, J., Althagafi, T.M., Ibrahim, E. H. Hamed A. Ghramh, Takwa E. Ellakwa, KH. S. Shaaban (2023). Characterization of Mechanical and Radiation Shielding Ability of CdO - SiO2 - B2O3 - MoO3 – LiF, Glasses. Silicon. https://doi.org/10.1007/s12633-023-02699-7.

[47] A. M. El-Khayatt (2010). Calculation of fast neutron removal cross-sections for some compounds and materials, Ann. Nucl. Energy. 37 218–222. https://doi.org/10.1016/j.anucene.2009.10.022.